

Solving PDEs with Unmeasurable Source Terms Using Coupled Physics-Informed Neural Network with Recurrent Prediction in Soft Sensor Modeling

Aina Wang, Pan Qin, Xi-Ming Sun, *Senior Member, IEEE*

Abstract—Nonhomogeneous partial differential equations (PDEs) are an applicable model in soft sensor modeling for describing spatiotemporal industrial systems with unmeasurable source terms, which cannot be well solved by existing physics-informed neural networks (PINNs). To this end, a coupled PINN (CPINN) with a recurrent prediction (RP) learning strategy (CPINN-RP) is proposed for soft sensor modeling in spatiotemporal industrial processes, such as vibration displacement. First, CPINN containing *NetU* and *NetG* is proposed. *NetU* is used to approximate the solutions to PDEs under study and *NetG* is used to regularize the training of *NetU*. The two networks are integrated into a data-physics-hybrid loss function. Then, we theoretically prove that the proposed CPINN has a satisfying approximation capacity to the PDEs solutions. Besides the theoretical aspects, we propose a hierarchical training strategy to optimize and couple the two networks to achieve the parameters of CPINN. Secondly, *NetU*-RP is achieved by *NetU* compensated by RP, the recurrently delayed output of CPINN, to further improve the soft sensor performance. Finally, simulations and experiment verify the effectiveness and practical applications of CPINN-RP.

Index Terms—Coupled physics-informed neural network, hierarchical training strategy, partial differential equations with unmeasurable source term, recurrent prediction, soft sensor,

I. INTRODUCTION

INDUSTRIAL processes have numerous variables, which are traditionally measured with hard sensors, like temperature sensor and displacement sensor. However, the limitations of the operational environment challenge most hardware sensors [1]. To tackle the problems, soft sensors are widely used to estimate the key variables using easy-to-measure variables and mathematical models [2], [3]. Partial differential equations (PDEs), such as the parabolic PDE type heat equation and the hyperbolic PDE type wave equation [4], [5], are one of the general representations for describing spatiotemporal dependence in physics [6], medicine [7], engineering [8], finance [9], and weather forecasting [10]. Thus, PDEs provide a feasible mathematical model candidate for soft sensor modeling techniques [11].

Numerical approaches, like the finite difference method (FDM) [12] and finite element method (FEM) [13], [14], have been widely investigated and used to solve PDEs and can ensure the feasibility of soft sensor. FDM used a topologically

square lines network to construct PDEs' discretization. However, complex geometries in multiple dimensions challenge FDM [15]. On the other hand, complex geometries can be treated with FEM [16]. The greatest difficulty of classical numerical approaches is the trade-off between the accuracy and efficiency caused by forming meshes.

Among the numerical methods, the Galerkin method is a famous computation method in which the linear combination of basis functions is employed to approximate the solutions to PDEs [17]. Furthermore, several works have used machine learning models to construct data-efficient and physics-informed learning methods for solving PDEs [9], [18]–[20]. Successful applications of deep learning methods in various fields, like image processing [21], text mining [22], and speech recognition [23], ensure that they are excellent replacers for solving PDEs [9]. Consequently, leveraging the well-known approximation capability of neural networks to solve PDEs is a natural idea and has been investigated in various forms previously [24]–[26]. The framework of physics-informed neural networks (PINNs) was introduced by [27] to solve PDEs with given initial and boundary conditions. Within the PINNs framework, both the sparse measurements and the physical knowledge were fully used [28]. The solution with respect to spatiotemporal dependence was obtained by minimizing the loss function [29]. Note that solving PDEs by machine learning and deep learning methods is usually mesh-free, which has no problem in balancing the efficiency and accuracy to form meshes.

PDEs can be classified into homogeneous and nonhomogeneous types. The homogeneous PDEs can describe systems without source terms. The nonhomogeneous PDEs can be used to reveal the continuous energy propagation behavior of the source and hereby are applicable for describing practical dynamical systems driven by source terms. The functional form of the solution and the source term were both assumed to be unknown in [30], in which the measurements of the source term can be obtained separately from the measurements of the solution. The recent work [31] can solve the PDEs with unknown source terms, where the source terms were assumed to be constant. Although the aforementioned methods have made great progress in solving the nonhomogeneous PDEs, independent measurements of the source terms in the operational domain cannot always be easily obtained from practical situations, like the heat source terms of the engines [32]. Furthermore, the existing methods with the assumption of the constant source terms cannot be extended to describe

The authors are with the Key Laboratory of Intelligent Control and Optimization for Industrial Equipment of Ministry of Education and the School of Control Science and Engineering, Dalian University of Technology, Dalian 116024, China e-mail: WangAn@mail.dlut.edu.cn, qp112cn@dlut.edu.cn, sunxm@dlut.edu.cn (*Corresponding author: Pan Qin*)

the spatiotemporal dependence of complex dynamical systems. Thus, the approximations to the solutions of PDEs with unmeasurable source terms under less prior information or without any prior information about source terms is an under-investigated issue.

To solve the PDEs with unmeasurable source terms for soft sensor modeling in spatiotemporal industrial processes, this research proposes a coupled-PINN (CPINN) with a recurrent prediction (RP) learning strategy (CPINN-RP), which is a two-phase learning strategy. In the first phase, CPINN containing *NetU* and *NetG* is proposed. *NetU* is used to approximate the solutions to PDEs under study and *NetG* is used to regularize the training of *NetU*. The two networks are integrated into a data-physics-hybrid loss function. Motivated by [33], a rigorous theoretical guarantee for the approximation capacity of CPINN is proven using the second power of the L^2 -norm in this work. Note that the recent work [34] also theoretically claimed the effective approximation of neural networks to the solutions of nonhomogeneous PDEs. However, our theory shows the upper bound of the approximation error of CPINN, which has not been considered in [34]. Besides the theoretical aspects, we also propose a hierarchical training strategy to optimize and couple the two networks for practical situations. If PDEs include the partial derivation of the temporal variable, the training dataset will be sampled with a fixed temporal interval. This discretization strategy can cause the defections of information. To this end, *NetU* is compensated by RP (*NetU-RP*) in the second phase and is further achieved with the recurrently delayed output of CPINN obtained in the first phase to improve the soft sensor performance. Finally, the numerical simulation and the physical experiments verify the effectiveness and practical applications of our proposed CPINN-RP in soft sensor modeling for spatiotemporal industrial processes with unmeasurable source terms.

The rest of the paper is organized as follows. The classical PINN is briefly reviewed in Section II. A two-phase learning strategy, CPINN-RP, is proposed in Section III. In the first phase, CPINN is used to approximate the solutions to PDEs under soft sensor modeling. In the second phase, *NetU-RP* is achieved to improve the soft sensor performance. In Section IV, our proposed CPINN-RP is verified with simulations and physical experiments. In Section V, the concluding remarks and the future work are presented.

II. BRIEF REVIEW OF PINNs

We first briefly review the basic idea of PINNs in computing data-driven solutions to the homogeneous PDEs [27], which are of the generalized form

$$u_t(\mathbf{x}, t) + \mathcal{N}[u(\mathbf{x}, t)] = 0, \quad \mathbf{x} \in \Omega \subseteq \mathbb{R}^d, \quad t \in [0, T] \subset \mathbb{R}. \quad (1)$$

Here, \mathbf{x} is the spatial variable; t is the temporal variable; $u : \mathbb{R}^d \times \mathbb{R} \rightarrow \mathbb{R}$ denotes the solution; $\mathcal{N}[\cdot]$ is a series of differential operators; the compact domain $\Omega \subseteq \mathbb{R}^d$ is a spatial bounded open set with the boundary $\partial\Omega$. PINNs are a neural network denoted by $\hat{u}(\mathbf{x}, t; \Theta_U)$, with Θ_U being the parameter, to approximate the solution satisfying (1).

PINNs can be trained by minimizing the loss function

$$\text{MSE}_H = \text{MSE}_{DH} + \text{MSE}_{PH}. \quad (2)$$

Here, MSE_{DH} is formulated as the following

$$\text{MSE}_{DH} = \frac{1}{\text{card}(D)} \sum_{(\mathbf{x}, t, u) \in D} (\hat{u}(\mathbf{x}, t; \Theta_U) - u(\mathbf{x}, t))^2, \quad (3)$$

where $\text{card}(\cdot)$ is the cardinality of set \cdot in this work, D is the training dataset, and $u(\mathbf{x}, t)$ can be obtained at (\mathbf{x}, t) . This mean-squared-error term (3) can be considered as the data-driven loss.

The left-hand-side of (1) can be used to define a residual function as the following

$$f(\mathbf{x}, t) = u_t(\mathbf{x}, t) + \mathcal{N}[u(\mathbf{x}, t)]. \quad (4)$$

Consequently, MSE_{PH} is formulated as the following

$$\text{MSE}_{PH} = \frac{1}{\text{card}(E)} \sum_{(\mathbf{x}, t) \in E} \hat{f}(\mathbf{x}, t; \Theta_U)^2, \quad (5)$$

where E denotes the set of collocation points, $\hat{f}(\mathbf{x}, t; \Theta_U)$ can be considered an approximation of the residual function $f(\mathbf{x}, t)$ based on $\hat{u}(\mathbf{x}, t; \Theta_U)$. $\hat{f}(\mathbf{x}, t; \Theta_U)$ obtained as the following

$$\hat{f}(\mathbf{x}, t; \Theta_U) = \hat{u}_t(\mathbf{x}, t; \Theta_U) + \mathcal{N}[\hat{u}(\mathbf{x}, t; \Theta_U)], \quad (6)$$

where $\hat{u}_t(\mathbf{x}, t; \Theta_U)$ and $\mathcal{N}[\hat{u}(\mathbf{x}, t; \Theta_U)]$ can be obtained using automatic differentiation [35]. MSE_{PH} is used to regularize $\hat{u}(\mathbf{x}, t; \Theta_U)$ to satisfy (1), which can be considered as the physics-informed loss for the homogeneous PDEs.

III. METHODS

A. Approximating Solutions to Nonhomogeneous PDEs

The nonhomogeneous PDEs under study are of the following generalized form

$$\begin{cases} u_t(\mathbf{x}, t) + \mathcal{N}[u(\mathbf{x}, t)] = g(\mathbf{x}, t), & \mathbf{x} \in \Omega, t \in [0, T] \\ \mathcal{B}[u(\mathbf{x}, t)] = g_b(\mathbf{x}, t), & \mathbf{x} \in \partial\Omega, t \in [0, T] \end{cases}, \quad (7)$$

where \mathbf{x} and t , Ω , $u : \mathbb{R}^d \times \mathbb{R} \rightarrow \mathbb{R}$, and $\mathcal{N}[\cdot]$ are similar to (1); $\mathcal{B}[\cdot]$ is the differential operator on the boundary. $g : \mathbb{R}^d \times \mathbb{R} \rightarrow \mathbb{R}$ and $g_b : \mathbb{R}^d \times \mathbb{R} \rightarrow \mathbb{R}$ denote the general types of source terms. In general, $g(\mathbf{x}, t)$ is the source term for dynamical systems and cannot always be easily measured in the interior of the operational domain owing to the limitations in practice, as mentioned in Section I. $g_b(\mathbf{x}, t)$ is a suitable source term active on $\partial\Omega$, which can be easily measured using sensors mounted on the surface [36].

The residual function is defined for the nonhomogeneous case as the following

$$\begin{cases} f_N(\mathbf{x}, t) = u_t(\mathbf{x}, t) + \mathcal{N}[u(\mathbf{x}, t)] - g(\mathbf{x}, t) = 0 \\ b_N(\mathbf{x}, t) = \mathcal{B}[u(\mathbf{x}, t)] - g_b(\mathbf{x}, t) = 0 \end{cases}. \quad (8)$$

When $g(\mathbf{x}, t)$ is exactly known, $f_N(\mathbf{x}, t)$ is obtained with automatic differentiation with respect to (8). However, the unmeasurable $g(\mathbf{x}, t)$ will lead to unknown $f_N(\mathbf{x}, t)$, which makes the aforementioned regularization (5) infeasible. To this end, CPINN is first proposed to approximate the solutions to PDEs with unmeasurable source terms in (7), which contains two neural networks: (a) *NetU* is for approximating the solution satisfying (7); (b) *NetG* is for regularizing the training of *NetU*.

To train CPINN, the training dataset is uniformly sampled from the systems governed by (7). The training dataset D is divided into $D = D_B \cup D_I$ with $D_B \cap D_I = \emptyset$, where D_B denotes the boundary and initial training datasets and D_I is the training dataset in the interior of Ω . Collocation points $(\mathbf{x}, t) \in E$ and $(\mathbf{x}, t) \in E_B$ correspond to those of $(\mathbf{x}, t, u) \in D_I$ and $(\mathbf{x}, t, u) \in D_B$, respectively. Then, we adopt the following data-physics-hybrid loss function

$$\text{MSE}_N = \text{MSE}_{DN} + \text{MSE}_{PN} \quad (9)$$

to train CPINN. MSE_{DN} and MSE_{PN} in (9) are the data-driven loss and physics-informed loss for the nonhomogeneous PDEs, respectively. MSE_{DN} adopts the following form

$$\text{MSE}_{DN} = \frac{1}{\text{card}(D)} \sum_{(\mathbf{x}, t, u) \in D_I \cup D_B} (\hat{u}(\mathbf{x}, t; \Theta_U) - u(\mathbf{x}, t))^2, \quad (10)$$

where $\hat{u}(\mathbf{x}, t; \Theta_U)$ is the function of $NetU$ with Θ_U being the parameter. MSE_{PN} is as the following

$$\begin{aligned} \text{MSE}_{PN} = & \frac{1}{\text{card}(E)} \sum_{(\mathbf{x}, t) \in E} (\hat{g}(\mathbf{x}, t; \Theta_G) - \hat{f}(\mathbf{x}, t; \Theta_U))^2 \\ & + \frac{1}{\text{card}(E_B)} \sum_{(\mathbf{x}, t) \in E_B} \hat{b}_N(\mathbf{x}, t; \Theta_U)^2, \end{aligned} \quad (11)$$

where $\hat{g}(\mathbf{x}, t; \Theta_G)$ is the function of $NetG$ with Θ_G being the parameter; $\hat{f}(\mathbf{x}, t; \Theta_U)$ has been defined by (6); $\hat{b}_N(\mathbf{x}, t; \Theta_U)$ can be considered an approximation of the residual function $b_N(\mathbf{x}, t)$ based on $\hat{u}(\mathbf{x}, t; \Theta_U)$. $\hat{b}_N(\mathbf{x}, t; \Theta_U)$ obtained as the following

$$\hat{b}_N(\mathbf{x}, t; \Theta_U) = \mathcal{B}[\hat{u}(\mathbf{x}, t; \Theta_U) - g_b(\mathbf{x}, t)].$$

MSE_{PN} is used to regularize the training of $NetU$ to satisfy the differential operators defined by $\mathcal{N}[\cdot]$ and $\mathcal{B}[\cdot]$ in (7).

B. Approximation Theorem for CPINN

Here, the approximation capacity of CPINN is theoretically proved based on the second power of L^2 -norm. The definition of well-posed PDE is first given as the following.

Definition 1 (Well-posed PDE). *PDE in (7) is called well-posed, if the following two conditions are satisfied: (a) there exists a unique solution for all functions $g(\mathbf{x}, t)$ and $g_b(\mathbf{x}, t)$ in (7); (b) for each pair-wised functions $\{g_1, g_{b1}\}$ and $\{g_2, g_{b2}\}$ satisfying (7), the corresponding solutions u_1 and u_2 satisfy*

$$\|u_1 - u_2\| \leq c \{\|g_1 - g_2\| + \|g_{b1} - g_{b2}\|\} \quad (12)$$

for some fixed and finite constant $0 < c \in \mathbb{R}$. Such a constant c is referred to as the Lipschitz constant of the PDE. Here, $\|\cdot\|$ denotes the L^1 norm.

Because $\hat{u}(\mathbf{x}, t; \Theta_U)$ and $\hat{g}(\mathbf{x}, t; \Theta_G)$ may not exactly satisfy (7), the following equation can be obtained:

$$\begin{cases} \hat{u}_t(\mathbf{x}, t; \Theta_U) + \mathcal{N}[\hat{u}(\mathbf{x}, t; \Theta_U)] = \hat{g}(\mathbf{x}, t; \Theta_G) + \hat{g}_d(\mathbf{x}, t; \Theta_G) + \hat{u}_d(\mathbf{x}, t; \Theta_U) \\ \mathcal{B}[\hat{u}(\mathbf{x}, t; \Theta_U)] = g_b(\mathbf{x}, t) + \hat{b}_N(\mathbf{x}, t; \Theta_U) \end{cases}, \quad (13)$$

where \hat{g}_d is the approximation error of $NetG$, \hat{u}_d and \hat{b}_N are the approximation error of $NetU$. In fact, the approximation

\hat{u} satisfies a PDE obtained by perturbing (7) with the approximation errors \hat{g}_d , \hat{u}_d , and \hat{b}_N .

For the generality of discussing the approximation ability of CPINN, instead of the mean squared error in (10) and (11), the second power of L^2 -norm is used as the following:

$$\hat{L}_{bound} = \int_0^T \int_{\partial\Omega} (\hat{u}_d(\mathbf{x}, t; \Theta_U)^2 + \hat{b}_N(\mathbf{x}, t; \Theta_U)^2) d\mathbf{x} dt \quad (14)$$

and

$$\hat{L}_{inter} = \int_0^T \int_{\Omega} \hat{g}_d(\mathbf{x}, t; \Theta_G)^2 d\mathbf{x} dt + \int_0^T \int_{\Omega} \hat{u}_d(\mathbf{x}, t; \Theta_U)^2 d\mathbf{x} dt, \quad (15)$$

Both (14) and (15) are assumed to have finite L^p -norm. Consequently, the loss function for CPINN is given as the following:

$$\hat{L}_{\hat{U}} = [T \text{card}(\Omega)]^{-1} \hat{L}_{inter} + [T \text{card}(\partial\Omega)]^{-1} \hat{L}_{bound} \quad (16)$$

The following theorem guarantees the approximation ability of CPINN to an exact solution to (7).

Theorem 1. *Assume PDE in (7) to be well-posed and the exact solution of it be given by u . Then, for any $\varepsilon > 0$, there exists a $\delta > 0$ such that for approximation \hat{u} obtained by CPINN,*

$$\hat{L}_{\hat{U}} < \delta \implies \|\hat{u} - u\| < \varepsilon.$$

Proof. According to Definition 1 and (13), there exists a finite Lipschitz constant c satisfying

$$\begin{aligned} & \|\hat{u}(\mathbf{x}, t; \Theta_U) - u(\mathbf{x}, t)\| \\ & < c \left\{ \left\| \left(\hat{g}(\mathbf{x}, t; \Theta_G) + \hat{g}_d(\mathbf{x}, t; \Theta_G) + \hat{u}_d(\mathbf{x}, t; \Theta_U) \right) \right. \right. \\ & \quad \left. \left. - \left(\hat{g}(\mathbf{x}, t; \Theta_G) + \hat{g}_d(\mathbf{x}, t; \Theta_G) \right) \right\| \right. \\ & \quad \left. + \left\| \left(g_b(\mathbf{x}, t) + \hat{b}_N(\mathbf{x}, t; \Theta_U) \right) - g_b(\mathbf{x}, t) \right\| \right\} \\ & = c \left\{ \left\| \hat{u}_d(\mathbf{x}, t; \Theta_U) \right\| + \left\| \hat{b}_N(\mathbf{x}, t; \Theta_U) \right\| \right\}. \end{aligned}$$

According to Hölder inequality, the bound of $\|\hat{u}_d\|$ is given as follows:

$$\begin{aligned} \|\hat{u}_d\| & \leq \left[\int_0^T \int_{\Omega \cup \partial\Omega} \hat{u}_d(\mathbf{x}, t; \Theta_U)^2 d\mathbf{x} dt \right]^{\frac{1}{2}} \left[\int_0^T \int_{\Omega \cup \partial\Omega} 1^2 d\mathbf{x} dt \right]^{\frac{1}{2}} \\ & = [T(\text{card}(\Omega \cup \partial\Omega))]^{\frac{1}{2}} \left[\int_0^T \int_{\Omega \cup \partial\Omega} \hat{u}_d(\mathbf{x}, t; \Theta_U)^2 d\mathbf{x} dt \right]^{\frac{1}{2}} \\ & \leq [T(\text{card}(\Omega) + \text{card}(\partial\Omega))]^{\frac{1}{2}} (\hat{L}_{inter} + \hat{L}_{bound})^{\frac{1}{2}} \end{aligned}$$

Then,

$$\begin{aligned} \|\hat{u}_d\|^2 & \leq T(\text{card}(\Omega) + \text{card}(\partial\Omega)) (\hat{L}_{inter} + \hat{L}_{bound}) \\ & = T^2(\text{card}(\Omega) + \text{card}(\partial\Omega)) \left(\frac{\text{card}(\Omega) \hat{L}_{inter}}{T \text{card}(\Omega)} + \frac{\text{card}(\partial\Omega) \hat{L}_{bound}}{T \text{card}(\partial\Omega)} \right) \\ & \leq T^2(\text{card}(\Omega) + \text{card}(\partial\Omega))^2 \hat{L}_{\hat{U}}, \end{aligned}$$

i.e.,

$$\|\hat{u}_d\| \leq T(\text{card}(\Omega) + \text{card}(\partial\Omega)) \hat{L}_{\hat{U}}^{\frac{1}{2}}.$$

Similarly, $\|\hat{b}_N\|$ can be proven to be bounded as follows:

$$\begin{aligned}
\|\hat{b}_N\| &\leq \left[\int_0^T \int_{\partial\Omega} \hat{b}_N(\mathbf{x}, t; \hat{\Theta}_U)^2 d\mathbf{x}dt \right]^{\frac{1}{2}} \left[\int_0^T \int_{\partial\Omega} 1^2 d\mathbf{x}dt \right]^{\frac{1}{2}} \\
&= (T \text{card}(\partial\Omega))^{\frac{1}{2}} \left[\int_0^T \int_{\partial\Omega} \hat{b}_N(\mathbf{x}, t; \hat{\Theta}_U)^2 d\mathbf{x}dt \right]^{\frac{1}{2}} \\
&\leq (T \text{card}(\partial\Omega))^{\frac{1}{2}} \hat{L}_{bound}^{\frac{1}{2}}.
\end{aligned}$$

Consequently,

$$\begin{aligned}
\|\hat{u} - u\| &< c \left\{ \|\hat{u}_d\| + \|\hat{b}_N\| \right\} \\
&\leq c \left\{ T(\text{card}(\Omega) + \text{card}(\partial\Omega)) \hat{L}_U^{\frac{1}{2}} + (T \text{card}(\partial\Omega))^{\frac{1}{2}} \hat{L}_{bound}^{\frac{1}{2}} \right\} \\
&= c \left\{ T(\text{card}(\Omega) + \text{card}(\partial\Omega)) \hat{L}_U^{\frac{1}{2}} + (T \text{card}(\partial\Omega))^{\frac{1}{2}} \left[\frac{\hat{L}_{bound}}{(T \text{card}(\partial\Omega))} \right]^{\frac{1}{2}} \right\} \\
&\leq c \left\{ T(\text{card}(\Omega) + \text{card}(\partial\Omega)) \hat{L}_U^{\frac{1}{2}} \right. \\
&\quad \left. + (T \text{card}(\partial\Omega)) \left[\frac{\hat{L}_{bound}}{(T \text{card}(\partial\Omega))} + \frac{\hat{L}_{inter}}{(T \text{card}(\Omega))} \right]^{\frac{1}{2}} \right\} \\
&\leq c \left\{ T(\text{card}(\Omega) + \text{card}(\partial\Omega)) \hat{L}_U^{\frac{1}{2}} + (T \text{card}(\partial\Omega)) \hat{L}_U^{\frac{1}{2}} \right\} \\
&= cT(\text{card}(\Omega) + 2\text{card}(\partial\Omega)) \hat{L}_U^{\frac{1}{2}}.
\end{aligned}$$

Finally, let

$$\delta = \frac{\varepsilon^2}{c^2 T^2 (\text{card}(\Omega) + 2\text{card}(\partial\Omega))^2}, \quad (17)$$

for which $\hat{L}_U < \delta$ yields

$$\|\hat{u} - u\| < cT(\text{card}(\Omega) + 2\text{card}(\partial\Omega)) \delta^{\frac{1}{2}} = \varepsilon. \quad \square$$

Because ε is a monotonically increasing function about δ in (17), $\varepsilon \rightarrow 0$ means $\delta \rightarrow 0$ and $\hat{u} \rightarrow u$. Based on Theorem 1, the following corollary can be further obtained.

Corollary 1. Let $\Theta_U \in \mathbb{R}^p$ and $\Theta_G \in \mathbb{R}^q$ denote the parameters of *NetU* $\hat{u}(\mathbf{x}, t; \Theta_U)$ and *NetG* $\hat{g}(\mathbf{x}, t; \Theta_G)$, respectively. Assume that $\hat{u} : \Omega \times [0, T] \rightarrow \mathbb{R}$ and $\hat{g} : \Omega \times [0, T] \rightarrow \mathbb{R}$ are continuous functions with respect to Θ_U and Θ_G , respectively. Then, for all $\delta > 0$, there exists $\{\Theta_U, \Theta_G\} \in \mathbb{R}^p \times \mathbb{R}^q$ satisfying

$$\hat{L}_U(\Theta_U, \Theta_G) < \delta.$$

Proof. The exact source term of (7) is given by g . Theorem 1 also implies that there exists a $\delta > 0$ for all $\varepsilon > 0$, such that

$$\hat{L}_U < \delta \implies \|\hat{g} - g\| < \varepsilon. \quad (18)$$

Note that $\hat{u}(\mathbf{x}, t; \Theta_U)$ and $\hat{g}(\mathbf{x}, t; \Theta_G)$ are continuous functions with respect to Θ_U and Θ_G , respectively. Furthermore, $\text{range}(\hat{u}) = \mathbb{R}$ and $\text{range}(\hat{g}) = \mathbb{R}$. Then, for any $\frac{\varepsilon}{2} > 0$, there exists Θ_U and Θ_G , it holds that

$$\|\hat{u} - u\| < \frac{\varepsilon}{2}, \quad \|\hat{g} - g\| < \frac{\varepsilon}{2}. \quad (19)$$

According to the second power of L^2 -norm (16), \hat{L}_U is a continuous function with respect to Θ_U and Θ_G . Consequently, the corollary holds. \square

Remark 1. Because $\mathbb{R}^{p \times q}$ is compact, Theorem 1 and Corollary 1 ensure that there exists a series of parameters $\{\Theta_U^{(j)}, \Theta_G^{(j)}\}$ to realize $\hat{L}_U(\Theta_U^{(j)}, \Theta_G^{(j)}) \rightarrow 0$ ($j \rightarrow \infty$). This fact

means that if CPINN is well trained to achieve $\{\Theta_U^{(j)}, \Theta_G^{(j)}\}$ using iterative optimization methods, *NetU* can approximate the solutions to the well-posed nonhomogeneous PDEs well.

C. Hierarchical Training Strategy

Considering the relation between *NetU* and *NetG* in CPINN, a hierarchical training strategy is proposed. Owing to the limitations of sensors, the exact functional forms or even sparse measurements of $g(\mathbf{x}, t)$ are not available. Thus, Θ_U and Θ_G should be iteratively estimated with mutual dependence. Before the hierarchical training strategy proceeds, some notations are introduced. Let $\hat{\Theta}_U^{(k)}$ denote the estimated parameter of *NetU* at k^{th} iteration step, $\hat{\Theta}_G^{(k+1)}$ denote the estimated parameter of *NetG* at $(k+1)^{\text{th}}$ iteration step, $\hat{\Theta}_U^{(k+1)}$ denote the estimated parameter of *NetU* at $(k+1)^{\text{th}}$ iteration step. Assuming k is the present iteration step, the core issue of the hierarchical training strategy is subsequently described by the following two optimization problems

$$\begin{aligned}
\hat{\Theta}_G^{(k+1)} &= \arg \min_{\Theta_G} \left\{ \text{MSE}_{DN}(\hat{\Theta}_U^{(k)}) + \text{MSE}_{PN}(\Theta_G; \hat{\Theta}_U^{(k)}) \right\} \\
&= \arg \min_{\Theta_G} \text{MSE}_{PN}(\Theta_G; \hat{\Theta}_U^{(k)})
\end{aligned} \quad (20)$$

and

$$\hat{\Theta}_U^{(k+1)} = \arg \min_{\Theta_U} \left\{ \text{MSE}_{DN}(\Theta_U) + \text{MSE}_{PN}(\Theta_U; \hat{\Theta}_G^{(k+1)}) \right\}. \quad (21)$$

The details of the hierarchical training strategy are described in Algorithm 1 and the architecture of CPINN is illustrated in Fig. 1. Furthermore, the iterative transmission of the param-

Algorithm 1 The hierarchical training strategy of optimizing and coupling for CPINN.

Initialization (Step 0)

The training dataset $(\mathbf{x}, t, u) \in D$ and collocation points $(\mathbf{x}, t) \in E$ are obtained with respect to sensors. Randomly generate parameters $\Theta_U^{(0)}$ and $\Theta_G^{(0)}$ for initializing *NetU* and *NetG*, respectively.

Step $k+1$: Assume $\hat{\Theta}_U^{(k)}$ and $\hat{\Theta}_G^{(k)}$ has been achieved at k^{th} iteration step.

while Stop Criterion is not satisfied do

Training for *NetG* by solving the optimization problem (20) to obtain $\hat{\Theta}_G^{(k+1)}$, where the estimations of $\hat{u}_t(\mathbf{x}, t; \hat{\Theta}_U^{(k)}) + \mathcal{N}(\hat{u}(\mathbf{x}, t; \hat{\Theta}_U^{(k)}))$ in MSE_{PN} is obtained from the former iteration result $\hat{\Theta}_U^{(k)}$. $\hat{\Theta}_G^{(k+1)}$ is used to regularize $\hat{f}(\mathbf{x}, t; \hat{\Theta}_U^{(k+1)})$ in MSE_{PN} at $(k+1)^{\text{th}}$ iteration step.

Training for *NetU* by solving the optimization problem (21) to obtain $\hat{\Theta}_U^{(k+1)}$, which is used to estimate $\hat{g}(\mathbf{x}, t; \hat{\Theta}_G^{(k+1)})$ in MSE_{PN} .

end while

Return the solution function $\hat{\Theta}_{U\text{-CPINN}} \rightarrow \hat{u}(\mathbf{x}, t; \hat{\Theta}_{U\text{-CPINN}})$, which can approximate the solution to (7) with any point (\mathbf{x}, t) in Ω .

eters of *NetG* and *NetU* happens in the hierarchical training strategy.

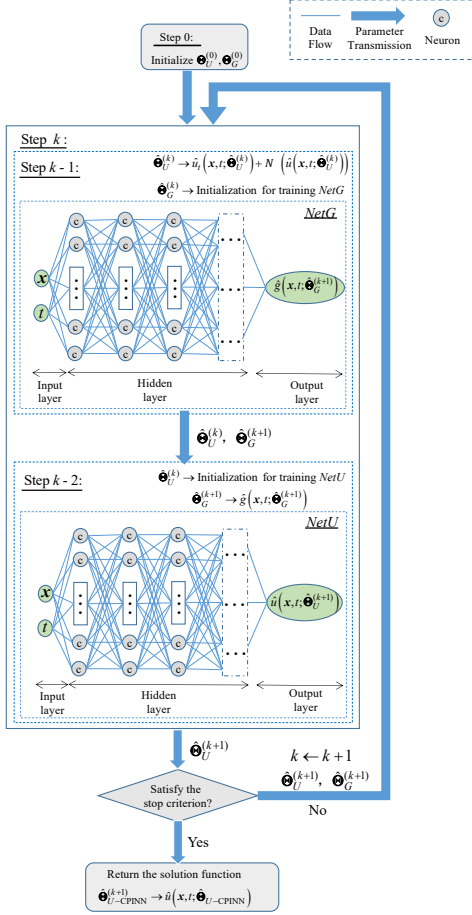


Fig. 1. CPINN's architecture diagram.

D. CPINN with RP Learning Strategy

If PDEs include partial derivation of temporal variables, the temporal dependencies in the measurements can be further used to improve the training efficiency. Note that the loss function (9) can be considered a Monte-Carlo approximation of the second power of L^2 -norm loss (16). The training datasets are sampled with a fixed temporal interval. This discretization strategy can cause the defections of information. For this reason, CPINN is followed by RP to obtain CPINN-RP to improve the performance of soft sensor, which contains a two-phase learning strategy: CPINN and RP in its first and second phases, respectively. In the first phase, CPINN containing *NetU* and *NetG* is proposed, and a hierarchical training strategy is used to optimize and couple the two networks to achieve well-trained parameter $\hat{\Theta}_{U-CPINN}$ to satisfy the PDEs for soft sensor modeling. In the second phase, *NetU* compensated by RP (*NetU-RP*) is initialized by $\hat{\Theta}_U^{(k)}$; the output $\hat{u}(\mathbf{x}, t; \hat{\Theta}_{U-CPINN})$ of CPINN obtained in the first phase can be recurrently delayed and fed to the *NetU-RP* as an alternative to observations when hardware sensors are unavailable [37]. The training strategy for *NetU-RP* is shown in Fig. 2. The same loss function that is previously used in (9) is also used to train the *NetU-RP* to achieve $\hat{u}(\mathbf{x}, t; \hat{\Theta}_{U-RP})$, i.e., the approximation $\hat{u}(\mathbf{x}, t)$.

IV. NUMERICAL EXPERIMENTS

In this section, CPINN-RP is verified with numerical simulations implemented with Pytorch. The fully-connected

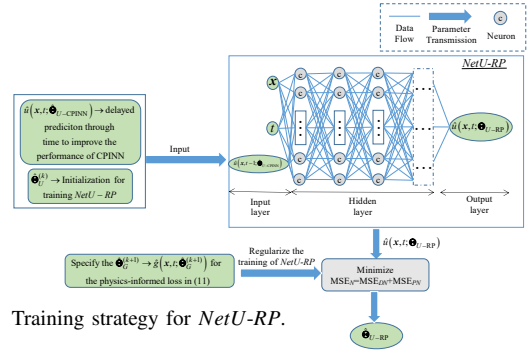


Fig. 2. Training strategy for *NetU-RP*.

neural networks with hyperbolic tangent activation functions are used (ensuring Theorem 1 and Corollary 1 hold) and are initialized by Xavier. In the first phase, L-BFGS [38] is used to hierarchically solve optimization problems (20) and (21) to couple *NetU* and *NetG* to achieve the parameter $\hat{\Theta}_{U-CPINN}$, which can be used to satisfy the solutions to PDEs with unmeasurable source terms for soft sensor modeling. In the second phase, *NetU-RP* is further achieved using the recurrently delayed output $\hat{u}(\mathbf{x}, t; \hat{\Theta}_{U-CPINN})$ to improve the soft sensor performance.

We evaluate the performance of our proposed CPINN-RP by means of root mean squared error (RMSE)

$$\text{RMSE} = \sqrt{\frac{1}{\text{card}(T_e)} \sum_{(\mathbf{x}, t, u) \in T_e} (\hat{u}(\mathbf{x}, t) - u(\mathbf{x}, t))^2},$$

where T_e is the testing dataset. $\hat{u}(\mathbf{x}, t)$ and $u(\mathbf{x}, t)$ denote the prediction and the corresponding ground truth, respectively. To further validate the performance of CPINN-RP, the Pearson's correlation coefficient (CC)

$$\text{CC} = \frac{\text{cov}(\hat{u}(\mathbf{x}, t), u(\mathbf{x}, t))}{\sqrt{\text{Var} \hat{u}(\mathbf{x}, t)} \sqrt{\text{Var} u(\mathbf{x}, t)}}$$

is also used to measure the similarity between prediction and ground truth, where $\text{cov}(\hat{u}(\mathbf{x}, t), u(\mathbf{x}, t))$ is the covariance of $\hat{u}(\mathbf{x}, t)$ and $u(\mathbf{x}, t)$, and $\text{Var} \hat{u}(\mathbf{x}, t)$ and $\text{Var} u(\mathbf{x}, t)$ are variances of $\hat{u}(\mathbf{x}, t)$ and $u(\mathbf{x}, t)$, respectively.

A. Case 1: Heat Equation With Unmeasurable Heat Source

The theory of heat equation was first developed for the purpose to model how a quantity such as heat diffusions through a given region, which has been widely used in various fields [39], [40]. CPINN-RP is first used to solve the following heat equation

$$\begin{cases} \frac{\partial u}{\partial t} = a^2 \frac{\partial^2 u}{\partial x^2} + g(x, t), & 0 < x < L, t > 0 \\ u|_{t=0} = \phi(x), & 0 \leq x \leq L \\ u|_{x=0} = 0, \quad \frac{\partial u}{\partial x} \Big|_{x=L} = 0, & t > 0 \end{cases}, \quad (22)$$

where the thermal diffusivity $a = 1$, the length of the bounded rod $L = \pi$, the initial temperature $\phi(x) = \sin(x/2)$, and the external heat source is $g(x) = \sin(x/2)$. The analytical solution $u(x, t)$ to (22) is obtained according to [41]. The above setup is used to generate the training and testing datasets. In practice, the source term is unmeasurable.

In this case, *NetU* is of three hidden layers consisting of 30 neurons individually; *NetG* is of eight hidden layers consisting of 20 units individually; *NetU-RP* is the same as *NetU*. A total of 130 training data in D_B , including 10 initial training data, 60 left boundary training data, and 60 right boundary training data are randomly sampled. Moreover, the 20 sparse collocation points are randomly sampled to enforce the structure of (22). The magnitude of the predictions $\hat{u}(x, t)$ using the above training dataset is shown in Fig. 3(a). Moreover, we compare the predictions and ground truths at fixed-time $t = 3$ and 7 in Fig. 3(b) and (c), respectively. Table I shows the evaluation criteria for the predictions obtained by CPINN-RP, respectively.

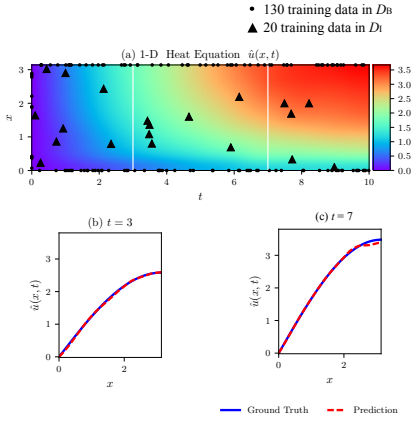


Fig. 3. (a) Predictions $\hat{u}(x, t)$ for the 1-D heat equation. (b) and (c) Comparisons of the predictions and ground truths correspond to the fixed-time $t=3$ and 7 snapshots depicted by the dashed vertical lines in (a), respectively.

TABLE I

EVALUATION CRITERIA FOR THE TEMPORAL SNAPSHOTS DEPICTED BY THE DASHED VERTICAL LINES IN FIG. 3-(A).

Criteria	3	7	$[0, \pi] \times [0, 10]$
RMSE	1.633733e-02	3.920911e-02	4.234160e-02
CC	9.999875e-01	9.999571e-01	9.999368e-01

B. Case 2: Wave Equation With Unmeasurable Driving Force

The wave equation is a second-order linear PDE for describing various fluctuation phenomena in nature [42], [43]. In this section, we further demonstrate CPINN-RP for soft sensor performance with the following wave equation

$$\begin{cases} \frac{\partial^2 u}{\partial t^2} = a^2 \frac{\partial^2 u}{\partial x^2} + g(x, t), & 0 < x < L, t > 0 \\ u|_{x=0} = 0, & u|_{x=L} = 0, & t > 0 \\ u|_{t=0} = 0, & \frac{\partial u}{\partial t}|_{t=0} = 0, & 0 \leq x \leq L \end{cases}, \quad (23)$$

where the wave speed a is 1, the length of bounded string L is π , the time of wave propagation t is 6, the external force is $g(x, t) = \sin \frac{2\pi x}{L} \sin \frac{2\pi t}{L}$. The analytical solution, training, and testing datasets are obtained similarly to Case 1.

In this experiment, *NetU* is of three hidden layers consisting of 30 neurons individually; *NetG* is of eight hidden layers consisting of 20 units individually; *NetU-RP* is the same as *NetU*. A total of 210 training data $(x, t, u(x, t))$ in D , including 50 initial training data, 120 boundary training data, and 40 training data in D_I are randomly sampled. Fig. 4(a) shows the

sparse training dataset and the magnitude of predictions $\hat{u}(x, t)$. Fig. 4(b) and (c) show the comparisons of the predictions and ground truths corresponding to the fixed-time $t=2$ and 4. The performance of CPINN-RP is further quantified in Table II.

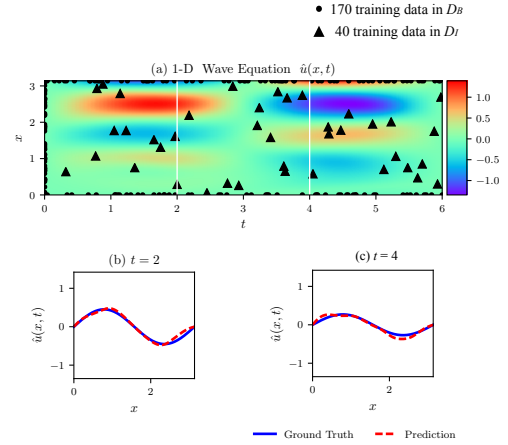


Fig. 4. (a) Predictions $\hat{u}(x, t)$ for 1-D wave equation. (b) and (c) Comparisons of the predictions and ground truths corresponding to the fixed-time $t=2$ and 4 snapshots depicted by the dashed vertical lines in (a), respectively.

TABLE II

EVALUATION CRITERIA FOR THE TEMPORAL SNAPSHOTS DEPICTED BY THE DASHED VERTICAL LINES IN FIG. 4-(A).

Criteria	2	4	$[0, \pi] \times [0, 6]$
RMSE	4.844044e-02	5.280401e-02	6.748852e-02
CC	9.898351e-01	9.819893e-01	9.876968e-01

V. EXPERIMENTAL VERIFICATION

In this section, to demonstrate the effectiveness of CPINN-RP in practical applications, the physical experiments are carried out based on the aero-engine involute spline couplings fretting wear experimental platform. The composition of the experiment system is presented in Fig. 5 and Fig. 6. As shown

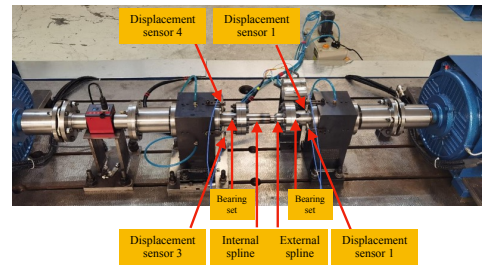


Fig. 5. Aero-engine involute spline couplings fretting wear experimental platform

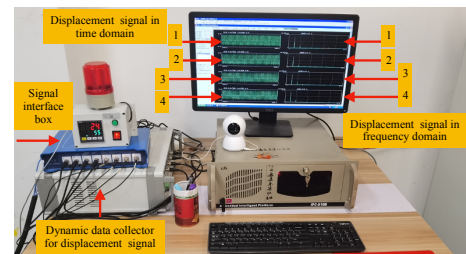


Fig. 6. Signal test system.

in Fig. 5, the experimental test bench is mainly composed of spline couplings, bearing sets, displacement sensors, and

a drive motor. The dataset is sampled with the condition as follows: (a) the working speed of the drive motor is 3000 r/min, (b) the sampling frequency is set to 2048Hz with 4096 sampling points. The sampled signals are shown in Fig. 7. The core of the system is to monitor the vibration

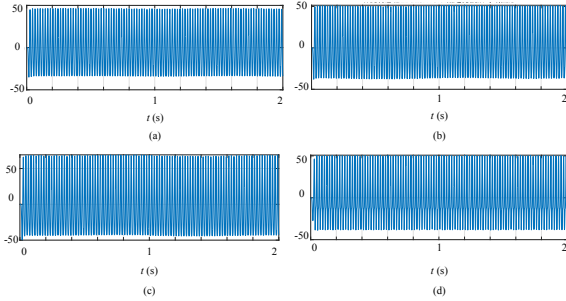


Fig. 7. Original displacement signals in time domain: (a) Signal obtained from sensor 1. (b) Signal obtained from sensor 2. (c) Signal obtained from sensor 3. (d) Signal obtained from sensor 4.

displacement of the internal and external spline shafts in the horizontal and vertical in the experiment. As described in Section IV, the vibration displacement of the spline shaft can be described in (23). The distance L between the shaft of two ends is 520mm, and displacements $u(x_i, t)$ for $i = 1, 2, 3, 4$ are measured by displacement sensors 1-4 as described in Fig. 5. The signal test system in Fig. 6 is developed to monitor the vibration signal. To verify the performance of CPINN-RT in soft sensor modeling, the measurement obtained by vibration displacement sensor 4 is unmeasurable to be assumed. The total of measurements is divided into training and testing datasets. Note that the total number of training dataset correspondings to about a mere 1% of the total available measurements. The settings of *NetU*, *NetG*, and *NetU-RP* can be referred to the Section IV. The performance of our proposed method is quantified in Table III. It further verifies

TABLE III
EVALUATION CRITERIA FOR THE PREDICTIONS OF THE SENSORS 4.

Sensor	Criteria	training	testing	$[0, 5.2] \times [0, 2]$
1	RMSE	2.613778e-02	5.776048e+00	5.772521e+00
	CC	9.999967e-01	9.879768e-01	9.879771e-01
2	RMSE	1.088167e-02	5.449913e+00	5.446586e+00
	CC	9.999997e-01	9.909315e-01	9.909329e-01
3	RMSE	9.480886e-03	4.762897e+00	4.759989e+00
	CC	9.999998e-01	9.933763e-01	9.933794e-01
4	RMSE	2.144921e+00	8.222315e+00	8.217437e+00
	CC	9.997592e-01	9.714094e-01	9.714027e-01

that the performance of soft sensor modeling using CPINN-RP is poorer compared to hardware sensors, however, it provides a reasonable alternative measurement when hardware sensors are unavailable.

VI. CONCLUSION

This work proposes a novel physics-informed neural networks called CPINN-RP for soft sensor, a two-phase learning strategy. In the first phase, CPINN containing *NetU* and *NetG* is proposed to approximate the solution, which is theoretically proven to have a satisfying approximation capacity for the solutions to the well-posed PDEs with unmeasurable source terms. Besides the theoretical aspects, the two networks are

optimized and coupled by the proposed hierarchical training strategy. In the second phase, *NetU-RP* is achieved with the recurrently delayed output of CPINN obtained in the first phase to further improve the soft sensor performance. Finally, the effectiveness and applications of CPINN-RP is validated with simulations and experiment. Our method can be expected to benefit the issue of soft sensor in spatiotemporal industrial system with unmeasurable source terms.

In the future, we will continue to use our CPINN-RP in more complex situations, like the structures of PDE are totally unknown. Feature extraction, like convolution and pooling, will be added to CPINN-RP for more widely applications. Besides, how to highly combine easy-to-measure variables and mathematical models will well benefit the performance of soft sensor.

REFERENCES

- [1] C. F. Lui, Y. Liu, and M. Xie, "A supervised bidirectional long short-term memory network for data-driven dynamic soft sensor modeling," *IEEE Transactions on Instrumentation and Measurement*, vol. 71, pp. 1–13, 2022.
- [2] K. Zhu and C. Zhao, "Dynamic graph-based adaptive learning for online industrial soft sensor with mutable spatial coupling relations," *IEEE Transactions on Industrial Electronics*, vol. 70, no. 9, pp. 9614–9622, 2023.
- [3] X. Jiang and Z. Ge, "Improving the performance of just-in-time learning-based soft sensor through data augmentation," *IEEE Transactions on Industrial Electronics*, vol. 69, no. 12, pp. 13716–13726, 2022.
- [4] Y. Tang, H. Su, T. Jin, and R. C. Flesch, "Adaptive pid control approach considering simulated annealing algorithm for thermal damage of brain tumor during magnetic hyperthermia," *IEEE Transactions on Instrumentation and Measurement*, 2023.
- [5] H. Karami, M. Azadifar, A. Mostajabi, P. Favrre, M. Rubinstein, and F. Rachidi, "Localization of electromagnetic interference sources using a time-reversal cavity," *IEEE Transactions on Industrial Electronics*, vol. 68, no. 1, pp. 654–662, 2021.
- [6] R. Pintelon, J. Schoukens, L. Pauwels, and E. Van Gheem, "Diffusion systems: stability, modeling, and identification," *IEEE Transactions on Instrumentation and Measurement*, vol. 54, no. 5, pp. 2061–2067, 2005.
- [7] C. Oszkinat, S. E. Luczak, and I. Rosen, "Uncertainty quantification in estimating blood alcohol concentration from transdermal alcohol level with physics-informed neural networks," *IEEE Transactions on Neural Networks and Learning Systems*, 2022.
- [8] J. Tu, C. Liu, and P. Qi, "Physics-informed neural network integrating pointnet-based adaptive refinement for investigating crack propagation in industrial applications," *IEEE Transactions on Industrial Informatics*, pp. 1–9, 2022.
- [9] J. Sirignano and K. Spiliopoulos, "Dgm: A deep learning algorithm for solving partial differential equations," *Journal of computational physics*, vol. 375, pp. 1339–1364, 2018.
- [10] K. Kashinath, M. Mustafa, A. Albert, J. Wu, C. Jiang, S. Esmaeilzadeh, K. Azizzadenesheli, R. Wang, A. Chattopadhyay, A. Singh et al., "Physics-informed machine learning: case studies for weather and climate modelling," *Philosophical Transactions of the Royal Society A*, vol. 379, no. 2194, p. 20200093, 2021.
- [11] X. Yuan, L. Li, Y. A. W. Shardt, Y. Wang, and C. Yang, "Deep learning with spatiotemporal attention-based lstm for industrial soft sensor model development," *IEEE Transactions on Industrial Electronics*, vol. 68, no. 5, pp. 4404–4414, 2021.
- [12] G. D. Smith, G. D. Smith, and G. D. S. Smith, *Numerical solution of partial differential equations: finite difference methods*. Oxford university press, 1985.
- [13] Z. Li, Z. Qiao, and T. Tang, *Numerical solution of differential equations: introduction to finite difference and finite element methods*. Cambridge University Press, 2017.
- [14] G. Dziuk and C. M. Elliott, "Finite element methods for surface pdes," *Acta Numerica*, vol. 22, pp. 289–396, 2013.
- [15] J. Peiró and S. Sherwin, "Finite difference, finite element and finite volume methods for partial differential equations," in *Handbook of materials modeling*. Springer, 2005, pp. 2415–2446.

- [16] J. N. Reddy, Introduction to the finite element method. McGraw-Hill Education, 2019.
- [17] X. Zhuang and C. Augarde, "Aspects of the use of orthogonal basis functions in the element-free galerkin method," International Journal for Numerical Methods in Engineering, vol. 81, no. 3, pp. 366–380, 2010.
- [18] S. Cuomo, V. S. Di Cola, F. Giampaolo, G. Rozza, M. Raissi, and F. Piccialli, "Scientific machine learning through physics-informed neural networks: Where we are and what's next," arXiv preprint arXiv:2201.05624, 2022.
- [19] N. Zobeiry and K. D. Humfeld, "A physics-informed machine learning approach for solving heat transfer equation in advanced manufacturing and engineering applications," Engineering Applications of Artificial Intelligence, vol. 101, p. 104232, 2021.
- [20] W. Chen, Q. Wang, J. S. Hesthaven, and C. Zhang, "Physics-informed machine learning for reduced-order modeling of nonlinear problems," Journal of computational physics, vol. 446, p. 110666, 2021.
- [21] M. Ye, J. Shen, G. Lin, T. Xiang, L. Shao, and S. C. Hoi, "Deep learning for person re-identification: A survey and outlook," IEEE transactions on pattern analysis and machine intelligence, vol. 44, no. 6, pp. 2872–2893, 2021.
- [22] R. Mondal, S. Bhowmik, and R. Sarkar, "tseggan: A generative adversarial network for segmenting touching nontext components from text ones in handwriting," IEEE Transactions on Instrumentation and Measurement, vol. 70, pp. 1–10, 2021.
- [23] A. Kamble, P. H. Ghare, and V. Kumar, "Deep-learning-based bci for automatic imagined speech recognition using spwvd," IEEE Transactions on Instrumentation and Measurement, vol. 72, pp. 1–10, 2023.
- [24] A. J. Meade Jr and A. A. Fernandez, "The numerical solution of linear ordinary differential equations by feedforward neural networks," Mathematical and Computer Modelling, vol. 19, no. 12, pp. 1–25, 1994.
- [25] I. E. Lagaris, A. Likas, and D. I. Fotiadis, "Artificial neural networks for solving ordinary and partial differential equations," IEEE transactions on neural networks, vol. 9, no. 5, pp. 987–1000, 1998.
- [26] I. E. Lagaris, A. C. Likas, and D. G. Papageorgiou, "Neural-network methods for boundary value problems with irregular boundaries," IEEE Transactions on Neural Networks, vol. 11, no. 5, pp. 1041–1049, 2000.
- [27] M. Raissi, P. Perdikaris, and G. E. Karniadakis, "Physics-informed neural networks: A deep learning framework for solving forward and inverse problems involving nonlinear partial differential equations," Journal of Computational physics, vol. 378, pp. 686–707, 2019.
- [28] M. Zhang, Q. Xu, and X. Wang, "Physics-informed neural network based online impedance identification of voltage source converters," IEEE Transactions on Industrial Electronics, vol. 70, no. 4, pp. 3717–3728, 2023.
- [29] Z. Mao, A. D. Jagtap, and G. E. Karniadakis, "Physics-informed neural networks for high-speed flows," Computer Methods in Applied Mechanics and Engineering, vol. 360, p. 112789, 2020.
- [30] M. Yang and J. T. Foster, "Multi-output physics-informed neural networks for forward and inverse pde problems with uncertainties," Computer Methods in Applied Mechanics and Engineering, p. 115041, 2022.
- [31] H. Gao, M. J. Zahr, and J.-X. Wang, "Physics-informed graph neural galerkin networks: A unified framework for solving pde-governed forward and inverse problems," Computer Methods in Applied Mechanics and Engineering, vol. 390, p. 114502, 2022.
- [32] L. Guzzella and C. Onder, Introduction to modeling and control of internal combustion engine systems. Springer Science & Business Media, 2009.
- [33] D. Van, C. Oosterlee, and A. Borovykh, "Optimally weighted loss functions for solving pdes with neural networks," Journal of Computational and Applied Mathematics, no. 405-, p. 405, 2022.
- [34] S. Stenen Blakseth, A. Rasheed, T. Kvamsdal, and O. San, "Combining physics-based and data-driven techniques for reliable hybrid analysis and modeling using the corrective source term approach," arXiv e-prints, pp. arXiv–2206, 2022.
- [35] A. G. Baydin, B. A. Pearlmutter, A. A. Radul, and J. M. Siskind, "Automatic differentiation in machine learning: a survey," Journal of Machine Learning Research, vol. 18, pp. 1–43, 2018.
- [36] D. Tang, F. Bi, J. Lin, X. Li, X. Yang, and X. Bi, "Adaptive recursive variational mode decomposition for multiple engine faults detection," IEEE Transactions on Instrumentation and Measurement, vol. 71, pp. 1–11, 2022.
- [37] X. Zhang and Z. Ge, "Local parameter optimization of lssvm for industrial soft sensing with big data and cloud implementation," IEEE Transactions on Industrial Informatics, vol. 16, no. 5, pp. 2917–2928, 2019.
- [38] C. Zhu, R. H. Byrd, P. Lu, and J. Nocedal, "Algorithm 778: L-bfgs-b: Fortran subroutines for large-scale bound-constrained optimization," ACM Transactions on mathematical software (TOMS), vol. 23, no. 4, pp. 550–560, 1997.
- [39] V. Bubanja, Y. Amagai, K. Okawa, and N.-H. Kaneko, "Mathematical modeling and measurement of low frequency characteristics of single-junction thermal converters," IEEE Transactions on Instrumentation and Measurement, vol. 71, pp. 1–4, 2022.
- [40] B.-C. Wang, H.-X. Li, and H.-D. Yang, "Spatial correlation-based incremental learning for spatiotemporal modeling of battery thermal process," IEEE Transactions on Industrial Electronics, vol. 67, no. 4, pp. 2885–2893, 2020.
- [41] B. R. Kusse and E. A. Westwig, Mathematical physics: applied mathematics for scientists and engineers. John Wiley & Sons, 2010.
- [42] Z. Liu, X. He, Z. Zhao, C. K. Ahn, and H.-X. Li, "Vibration control for spatial aerial refueling hoses with bounded actuators," IEEE Transactions on Industrial Electronics, vol. 68, no. 5, pp. 4209–4217, 2021.
- [43] N. Chu, Y. Ning, L. Yu, Q. Liu, Q. Huang, D. Wu, and P. Hou, "Acoustic source localization in a reverberant environment based on sound field morphological component analysis and alternating direction method of multipliers," IEEE Transactions on Instrumentation and Measurement, vol. 70, pp. 1–13, 2021.